Desalination and Water Treatment
www.deswater.com
doi: 10.5004/dwt.2023.30001

311 (2023) 155–161
November

Magnetic modified chitosan composites for hexavalent chromium removal

Bangchang Wei[a,†], Zheng Ji[a,†], Ya Xu[a], Shengnan Kong[a], Yansong Zhang[a], Chuanrun Li[a,b,*], Huchuan Wang[a,b,*]

[a]*Department of Medicinal Chemistry, School of Pharmacy, Anhui University of Chinese Medicine, Hefei, Anhui 230012, China, emails: crli@ahtcm.edu.cn (C.R. Li), WHC03231986@163.com (H.C. Wang)*
[b]*Anhui Province Key Laboratory of Pharmaceutical Preparation Technology and Application, Anhui University of Chinese Medicine, Hefei, Anhui 230012, China*

Received 6 July 2023; Accepted 26 September 2023

ABSTRACT

In this paper, we successfully prepared magnetic modified chitosan composites by mixing hydroxyapatite with polypropylene glycol modified chitosan and wrapping magnetic nanoparticles. The adsorption study of Cr(VI) revealed that the adsorption process was more in accordance with the pseudo-second-order kinetic and followed the Langmuir isotherm adsorption process, which indicated that the adsorption process was monolayer adsorption, and the fitted calculations showed that the maximum adsorption capacity of Cr(VI) was 795.14 mg·g^{-1}. Thermodynamic model reflected that the adsorption process was spontaneous heat absorption.

Keywords: Modified chitosan; Composites; Adsorption; Hexavalent chromium

1. Introduction

Chromium (Cr) is generally derived from electroplating, mining, leather tanning, dyestuff and other industries [1]. Cr mainly exists in the valence states +3 and +6, Cr(III) is an essential trace element in human body, which can promote growth and development, regulate blood glucose and protect cardiovascular system [2,3]. However, Cr(VI) is toxic, it is 500 times more toxic than Cr(III), and is capable of producing single electron transfer in the body, inducing gene mutation and causing flat epithelial cancer, adenocarcinoma and lung cancer with long-term intake [4,5].

Adsorption is a good method to deal with heavy metal contamination, and the effectiveness of adsorption is inseparable from the nature of the adsorbent. Chitosan (CS), natural adsorbent rich in hydroxyl and amino groups, has been reported in previous studies and modified in different ways to enhance mechanical properties, acid resistance and adsorption capacity [6,7]. However, there is still a need for continued research on the modification of CS. Polypropylene glycol (PPG) is a widely used fixative that enhances the stability of copolymer structures, and grafting to CS surface not only increases the mechanical strength but also can introduce a large number of functional groups [8,9]. If only a simple modification of the structure is performed, it may already be difficult to meet the treatment requirements of emerging contaminants. Hydroxyapatite (HAP) is a phosphate inorganic salt, non-toxic, non-hazardous, biocompatibility, and the calcium ions in the unit cell are easily exchanged with other metal ions [10]. However, HAP itself is easily agglomerated, which greatly reduces the adsorption performance of HAP [11]. Considering the existence of a large number of voids inside the modified chitosan, it may be an ideal solution for the agglomeration of HAP itself if HAP is doped into the voids. In order to avoid the problem of incomplete recovery of adsorbent after use, we introduced magnetic nanoparticles Fe_3O_4 to facilitate the rapid separation of adsorbent by external magnetic field at the end of adsorption and prevent secondary contamination. Nano Fe_3O_4 has been successfully applied to the treatment of Cr(VI) polluted water. Fe(II) can reduce Cr(VI) to

* Corresponding author.

Cr(III) [12,13]. Herein, we prepared, characterized and tested the modified chitosan composites Fe_3O_4-SiO_2@PPG-MA-CS-HAP and the adsorption capacity of adsorbent FS@PMCH for Cr(VI) was studied.

2. Materials and methods

2.1. Chemicals

CS (Mw = 30,000), $CaCl_2$ (≥96.0%), H_3PO_4 (≥85%), $K_2Cr_2O_7$ (≥99%) were purchased from Sinopharm Chemical Reagent Co., Ltd., (Shanghai, China). PPG600, Fe_3O_4 (≥99.5%, 200 nm), tetraethyl orthosilicate (≥98%), glutaraldehyde (50%), diphenylcarbazide (AR) and sodium tripolyphosphate (STPP, purity ≥98%) were purchased from Macklin Biochemical Technology Co., Ltd., (Shanghai, China). 4-Dimethylaminopyridine (DMAP, purity ≥ 99%) and maleic anhydride (MA, purity ≥ 99.5%) were purchased from Shanghai Aladdin Reagent Co., Ltd.

2.2. Synthesis of the Fe_3O_4-SiO_2@PPG-MA-CS-HAP (FS@PMCH) adsorbent adsorbent

PMC were synthesized according to the previous work [9]. Our research group successfully synthesized FS@PMCH before [14]. Add calcium chloride and phosphoric acid solution to the PMC solution dropwise at the same time (keep the calcium-phosphorus ratio at 1.67), stir rapidly, and adjust the pH of the solution to be weakly basic with hydrochloric acid and sodium bicarbonate. After dropwise addition, stir slowly for 4 h, age for 24 h and mix with already prepared Fe_3O_4-SiO_2, sonicate for 30 min, stir mechanically at 30°C for 2 h, then add glutaraldehyde and stir at 60°C for 1 h. At the end of the reaction, separate by external magnetic field, wash several times with anhydrous ethanol and ultrapure water, dry under vacuum at 50°C to obtain FS@PMCH powder for use [15–17].

2.3. Adsorption experiment

Weigh a certain amount of adsorbent in a conical flask, add Cr(VI) solution with a certain pH, shake at constant temperature, and determine the remaining Cr(VI) concentration in the solution by diphenylcarbazide method when the adsorption is equilibrium. Each group of experiments was repeated three times. The adsorption capacity (Q_e, mg·g^{-1}) was calculated in Eq. (1):

$$Q_e = \frac{\left(C_0 - C_e\right) \times V}{m} \tag{1}$$

where C_0 (mg·L^{-1}) is the initial concentration; C_e (mg·L^{-1}) is the equilibrium concentration; V (L) is the solution volume; m (g) is the weight of the adsorbent.

2.4. Characterization

Scanning electron microscopy (SEM, TESCAN MIRA4, Czech) was used to analyze the apparent topography. X-ray photoelectron spectroscopy (XPS) spectra were obtained by an X-ray diffractometer (Bruker D8 ADVANCE, Germany). Fourier-transform infrared spectroscopy (FTIR, Thermo Fisher Nicolet is50, USA) was used to evaluate the distribution of functional groups on the surface.

3. Results and discussion

3.1. Characterization of FS@PMCH

The microscopic morphology of FS@PMCH can be observed by SEM. As shown in Fig. 1, Fe_3O_4 presents an obvious spherical structure, which is not perfect but still a three-dimensional structure. After introducing magnetic Fe_3O_4, clear spherical structures also appear in the microstructure of the adsorbent FS@PMCH, and some of the spherical structures have a larger volume relative to the original Fe_3O_4, which indicates the successful preparation of magnetic composites.

Our group has previously carried out FTIR, thermogravimetric analysis, X-ray diffraction (XRD) and magnetic hysteresis loops (VSM) analysis of FS@PMCH. As for FTIR, the spectrum of FS@PMCH contains the related absorption peaks of PMCH (2,871; 1,030 and 900 cm^{-1}) and FS (790 and 558 cm^{-1}), indicating that the magnetic nanoparticles are successfully doped in PMCH. As for XRD, the characteristic peaks of the Fe_3O_4 structure appear in the sample spectrum, indicating that the structure of Fe_3O_4 in FS@PMCH is not significantly affected. FS@PMCH has the lowest mass loss rate from room temperature to 800°C compared to CS and PMCH. The saturation magnetization of FS@PMCH is significantly lower than that of uncomposited Fe_3O_4, but FS@PMCH can be quickly separated under an external magnetic field [14].

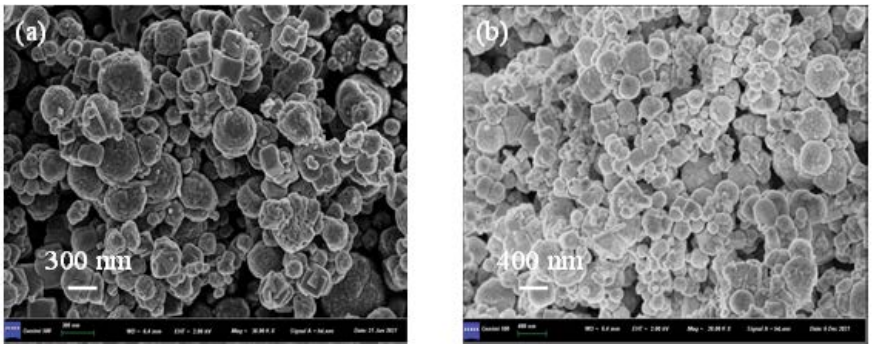

Fig. 1. Scanning electron micrographs: (a) Fe_3O_4 and (b) FS@PMCH.

The FTIR spectrum is shown in Fig. 2. FS@PMCH has a smooth and broad peak at 3,310 cm^{-1}, which belongs to the stretching vibration of –OH. After adsorption of Cr(VI), the stretching vibration peak of –OH shifted to 3,397 cm^{-1} and the absorption peak became stronger and wider. It indicates that –OH may play a role in the adsorption of Cr(VI) [18].

FS@PMCH has an absorption peak at 556 cm^{-1}, confirming the presence of Fe_3O_4. After the adsorption of Cr(VI), the 556 cm^{-1} peak shifted to 578 cm^{-1}, indicating that Fe_3O_4 was involved in the adsorption process. After adsorption, two new peaks can be observed at 1,420 and 1,563 cm^{-1}, which belong to the stretching vibration of $Cr(OH)_3$. The absorption peak of FS@PMCH at 1,032 cm^{-1} belongs to the stretching vibration of PO_4^-, but after adsorbing Cr(VI), the peak here shifts to 1,065 cm^{-1} and the peak becomes wider and stronger, which may be related to the stretching vibration of adsorbed CrO_4^{2-} [19]. These indicated that Cr(VI) was successfully adsorbed on the adsorbent FS@PMCH, and part of Cr(VI) was oxidized to Cr(III).

3.2. Effect of pH on adsorption capacity

pH is an important factor affecting the adsorption capacity, mainly because pH not only changes the nature of the functional groups on the adsorbent surface but also affects the form of heavy metal ions present [20]. At different solution pH, Cr(VI) exists in different ionic forms, such as: $HCrO_4^-$, CrO_4^{2-}, $Cr_2O_7^{2-}$. When pH < 4, Cr(VI) mainly exists in the form of $HCrO_4^-$ [21]. It can be seen that the adsorption capacity of Cr(VI) increases and then decreases as the pH increases from 1 to 5 in Fig. 3. When the solution pH = 2, the adsorption capacity is the largest. We consider that there is some damage to the adsorbent material itself when the solution acidity is too high, which leads to a relatively low adsorption capacity; furthermore, the degree of protonation of functional groups on the adsorbent surface gradually decreases with the increase of pH, and the electrostatic interaction with Cr(VI) decreases, which leads to a decrease in the adsorption capacity of Cr(VI) [22,23].

3.3. Effect of time on adsorption capacity

The effect of time can reflect the length of time taken to reach equilibrium adsorption of a unit weight of adsorbent in a certain concentration of heavy metal solution. From Fig. 4 it can be seen that the adsorption capacity grows very fast within 1 h, slowly within 1–2 h, and almost constant after 2 h, which reflects the fact that the active sites in the adsorbent are gradually occupied as time increases until there are no effective adsorption sites to occupy. Immediately afterwards, kinetic simulations of the adsorption data were performed to further investigate the adsorption process, and the kinetic equations in non-linear.

Pseudo-first-order kinetic model:

$$Q_t = Q_e \times \left(1 - e^{-k_1 t}\right) \tag{2}$$

Pseudo-second-order kinetic model:

$$Q_t = \frac{Q_e^2 k_2 t}{1 + k_2 Q_e t} \tag{3}$$

Elovich kinetic model:

$$Q_t = \beta \times \ln\left(\alpha\beta t\right) \tag{4}$$

where Q_t (mg·g^{-1}) is the adsorption capacity at time t; k_1 (min^{-1}) is the rate constant of the pseudo-first-order kinetic model; k_2 (g·mg^{-1}·min^{-1}) is the rate constant of the pseudo-second-order kinetic model; α (mg·g^{-1}·min^{-1}) is the rate constant of Elovich kinetic model; β (g·mg^{-1}) is the desorption constant of Elovich model.

From the kinetic model parameters in Table 1, it can be seen that the correlation coefficient (R^2) values of the pseudo-second-order kinetic model are higher than the other

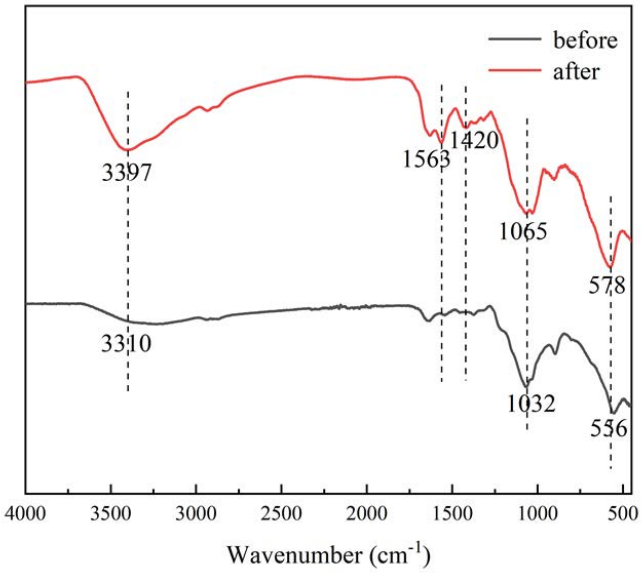

Fig. 2. Fourier-transform infrared spectroscopy of FS@PMCH before and after adsorption of Cr(VI).

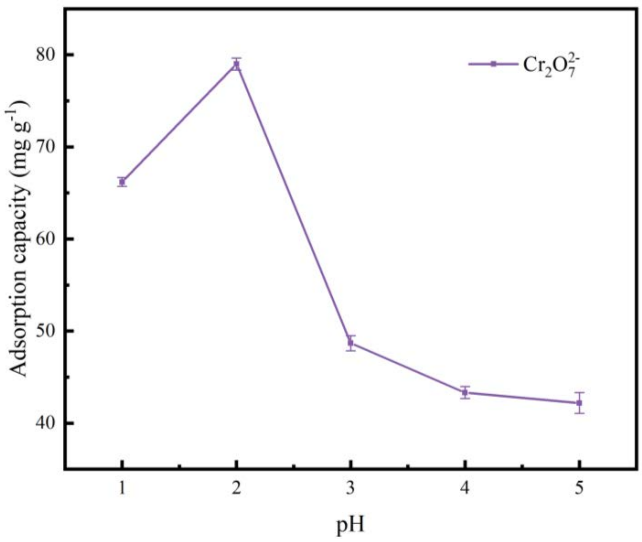

Fig. 3. Effect of pH on adsorption capacity (adsorption conditions: adsorbent = 25 mg, Cr(VI) = 100 mg·L^{-1}, t = 2 h, T = 298.15 K).

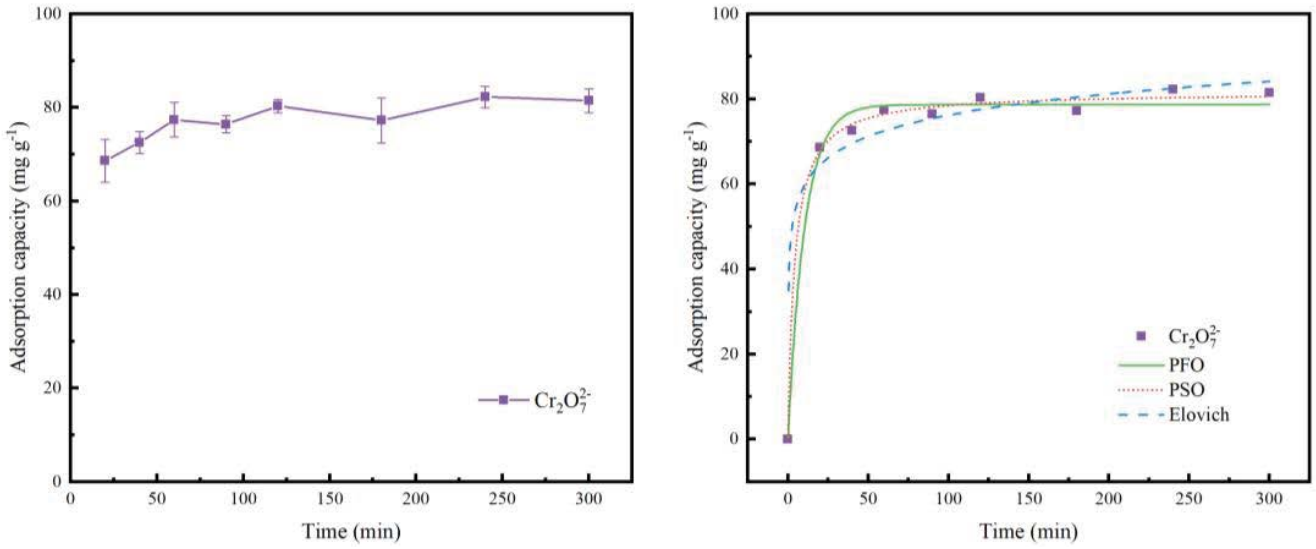

Fig. 4. Effect of time on adsorption capacity and adsorption kinetics of FS@PMCH (adsorption conditions: adsorbent = 25 mg, pH = 2, Cr(VI) = 100 mg·L^{-1}, T = 298.15 K).

Table 1
Adsorption kinetics model parameters of FS@PMCH

Type of models	Cr(VI)
Pseudo-first-order model	
Q_e (mg·g^{-1})	78.67
k_1 (min^{-1})	0.0965
R^2	0.9901
Pseudo-second-order model	
Q_e (mg·g^{-1})	81.66
k_2 (g·mg^{-1}·min^{-1})	3 × 10^{-3}
R^2	0.9963
Elovich model	
α (mg·g^{-1}·min^{-1})	7.2272
β (g·mg^{-1})	52.45
R^2	0.8092

kinetic models, which indicates that the pseudo-second-order kinetic model is more suitable for handling the adsorption experimental data [24].

3.4. Effect of initial concentration on adsorption capacity

The adsorption isotherm is an important way to measure the relationship between the initial concentration of a contaminant and the adsorption capacity. Here, two isotherm models are used to analyze the data and to investigate the mechanisms that exist for the adsorption process. The equations in nonlinear are as follows:

Langmuir model:

$$Q_e = \frac{Q_m K_L C_e}{1 + K_L C_e} \quad (5)$$

Table 2
Adsorption isotherms model parameters of FS@PMCH

Type of models	Cr(VI)		
	298.15 K	308.15 K	318.15 K
Langmuir model			
Q_m (mg·g^{-1})	795.14	817.74	1,152.63
K_L (L·mg^{-1})	0.0024	0.0034	0.0028
R^2	0.9713	0.9850	0.9846
Freundlich model			
$1/n$	0.7774	0.7385	0.7949
K_F (mg$^{(1-1/n)}$·L$^{1/n}$·g^{-1})	4.1704	6.5646	6.2172
R^2	0.9707	0.9838	0.9822

Freundlich model:

$$Q_e = K_F C_e^{1/n} \quad (6)$$

where Q_m (mg·g^{-1}) is the maximum adsorption capacity; K_L (L·mg^{-1}) is the constant of Langmuir model; K_F (mg$^{(1-1/n)}$·L$^{1/n}$·g^{-1}) is the constant of Freundlich model; n is the Freundlich heterogeneity factor.

In Table 2, the R^2 of the Langmuir model is slightly higher than that of the Freundlich model, which indicates that the adsorption of Cr(VI) by FS@PMCH is mainly monolayer-based, and the maximum adsorption capacity calculated from the fitted data is significantly better than that previously reported (as shown in Table 3) [25]. The Langmuir model is a theoretical model, which assumes a fixed number of active sites on the surface of the adsorbent [26]. When the concentration of adsorbate is low, there are more idle active sites. As the concentration of pollutants increases, more active sites are used and the adsorption capacity increases. When the concentration of the pollutant

increases to a certain extent, the active site of the adsorbent is completely occupied, and the adsorption capacity will not increase with the increase of the concentration of the pollutant, and the adsorption capacity reaches the platform period from the rising period. In this experiment, the concentration of pollutants did not reach the platform period. Therefore, the maximum adsorption capacity measured by the experiment is quite different from the maximum adsorption capacity of the Langmuir model.

3.5. Effect of temperature on adsorption capacity

The effect of temperature on the adsorption capacity was investigated on the basis of exploring the relationship between the initial concentration of contaminant and the adsorption capacity, and a preliminary analysis of the thermodynamic parameters was performed. The thermodynamic parameters were formulated using Eqs. (7)–(9) [32–34]:

$$\Delta G^\circ = -RT \times \ln K \tag{7}$$

$$\ln K = \frac{\Delta S^\circ}{R} - \frac{\Delta H^\circ}{RT} \tag{8}$$

$$K = K_L \times M_{ad} \times 10^3 \times 55.5 \tag{9}$$

where R (8.314 J·mol^{-1}·K^{-1}) is the universal gas constant; T (K) is the absolute temperature; M_{ad} is the relative molecular mass of the contaminant.

In Table 4, it can be seen that ΔG° is negative at different temperatures and ΔG° decreases with increasing temperature, which indicates that the adsorption process of Cr(VI) is spontaneous and the higher the temperature is in favor of the adsorption of Cr(VI) within a certain temperature range. A positive value of ΔH° indicates that the adsorption process is heat-absorbing and also proves that it is dominated by chemisorption. A positive value of ΔS° indicates that the contact between the adsorbent and the adsorbent solid–liquid interface is more random [35,36].

Table 3
Adsorption capacity of Cr(VI) by different adsorbents

Adsorbents	Adsorption capacity (mg·g^{-1})	References
CYPH@IL101/ chitosan capsule	104.38	[2]
CMBB	127	[25]
SBMGO	142.85	[27]
MCC-PVIM-4	134.1	[28]
PPF@PANI+PPy	510.9	[29]
AC/ACI	154.56/241.55	[26]
Fe_3O_4 NPs	56.625	[30]
Chitosan	128.0	[31]
FS@PMCH	795.14	This study

3.6. Adsorption mechanism

In Fig. 6a the characteristic peak of metal Cr can be observed after adsorption of Cr(VI), indicating the adsorption of Cr on the surface of the adsorbent. Fig. 6b shows the high resolution XPS spectra of Cr 2p after adsorption. The peak with high binding energy is Cr 2p 1/2 and the

Table 4
Thermodynamic parameters of FS@PMCH

Contaminant	Temperature (K)	ΔG (kJ·mol^{-1})	ΔH (kJ·mol^{-1})	ΔS (J·mol^{-1}·K^{-1})
Cr(VI)	298.15 K	–25.45	26.61	174.60
	308.15 K	–27.20		
	318.15 K	–27.66		

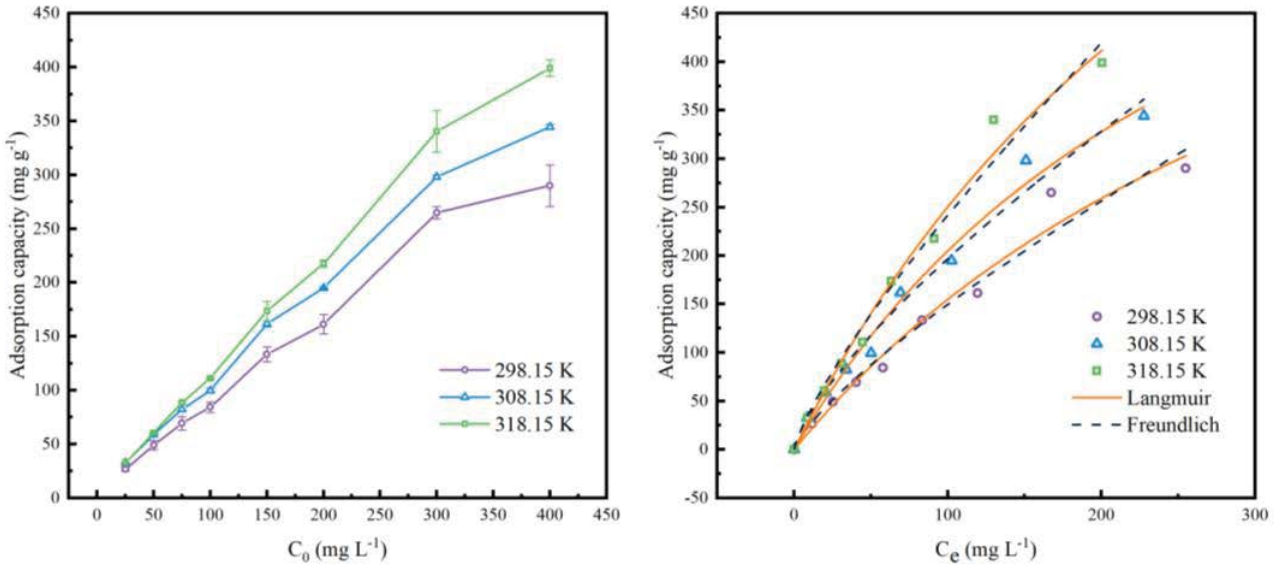

Fig. 5. Effect of initial concentration on adsorption capacity and adsorption isotherms of FS@PMCH (adsorption conditions: adsorbent = 25 mg, pH = 2, t = 2 h).

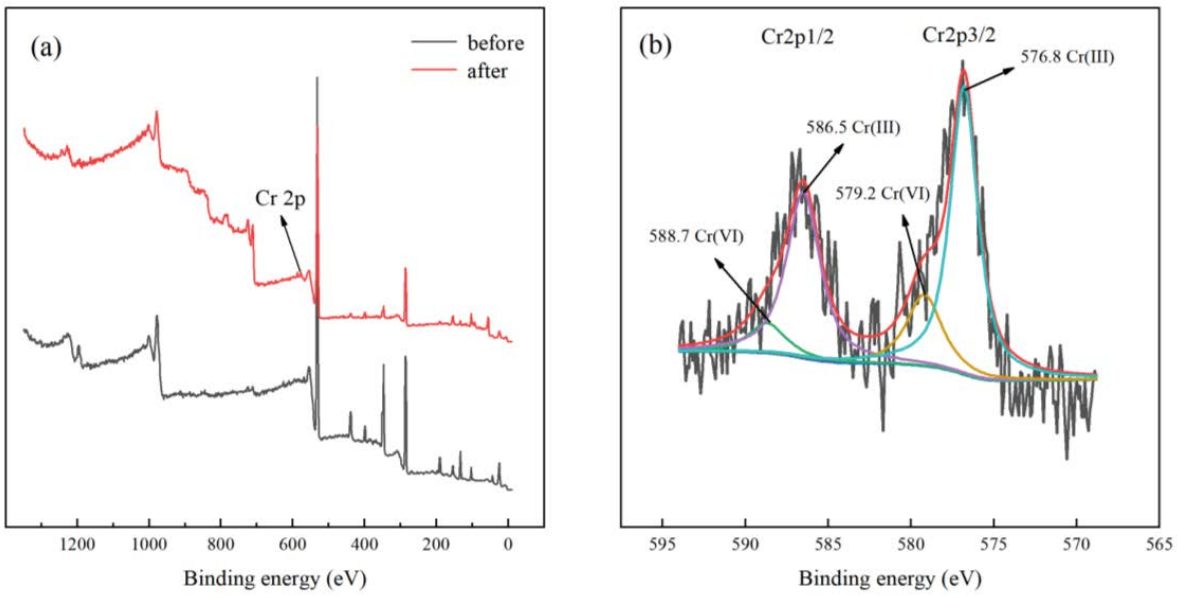

Fig. 6. X-ray photoelectron spectroscopy survey spectrum (a) of FS@PMCH before and after adsorption and (b) of Cr 2p high-resolution spectra.

peak with low binding energy is Cr 2p 3/2. Some of the hexavalent Cr adsorbed on the surface is oxidized to trivalent Cr. This may be promoted by the carboxyl groups on the surface of the adsorbent [37].

4. Conclusion

In this study, we prepared magnetic modified chitosan composites by a relatively simple synthetic method and demonstrated the successful preparation of magnetic modified chitosan composites using various characterization methods. The effects of different factors on the adsorption capacity were discussed and the best experimental factors were selected. In addition, kinetics, isothermals and thermodynamic analyses were performed for the experimental data, and the results confirmed that the adsorption process is dominated by spontaneous monolayer chemisorption, indicating that the adsorbent FS@PMCH is promising for certain applications.

Acknowledgement

This work was supported by the National Key Research and Development Program of China and [No. 2022YFB3805102]; the Natural Science Foundation of Anhui Province [No. 1808085QH289]; the Key Project of Natural Science Research of Anhui Universities [No. KJ2020A0432]; and the Quality Project of Higher Education in Anhui Province [No. 2020xfxm35].

Declaration of interest statement

The authors declare that they have no known competing financial interests or personal relationships that could have appeared to influence the work reported in this paper. Bangchang Wei and Zheng Ji contributed equally to this manuscript.

Data availability statement

The data that support the findings of this study are available from the corresponding author, upon reasonable request.

References

[1] M. Bhaumik, S. Agarwal, V.K. Gupta, A. Maity, Enhanced removal of Cr(VI) from aqueous solutions using polypyrrole wrapped oxidized MWCNTs nanocomposites adsorbent, J. Colloid Interface Sci., 470 (2016) 257–267.
[2] X. Lin, J. Liu, S. Wan, X. He, L. Cui, G. Wu, A novel strategy for Cr(VI) removal from aqueous solution via CYPH@IL101/chitosan capsule, Int. J. Biol. Macromol., 136 (2019) 35–47.
[3] J.B. Lu, K. Xu, J.M. Yang, Y.R. Hao, F. Cheng, Nano iron oxide impregnated in chitosan bead as a highly efficient sorbent for Cr(VI) removal from water, Carbohydr. Polym., 173 (2013) 28–36.
[4] S.U. Din, M.S. Khan, S. Hussain, M. Imran, S. Haq, M. Hafeez, A. Zainul, F.U. Rehman, X.N. Chen, Adsorptive mechanism of chromium adsorption on siltstone-nanomagnetite-biochar composite, J. Inorg. Organomet. Polym. Mater., 31 (2021) 1608–1620.
[5] N. Hayashi, D. Matsumura, H. Hoshina, Y. Ueki, T. Tsuji, J. Chen, N. Seko, Chromium(VI) adsorption–reduction using a fibrous amidoxime-grafted adsorbent, Sep. Purif. Technol., 277 (2021) 119536, doi: 10.1016/j.seppur.2021.119536.
[6] W.S.W. Ngah, L.C. Teong, M.A.K.M. Hanafiah, Adsorption of dyes and heavy metal ions by chitosan composites: a review, Carbohydr. Polym., 83 (2011) 1446–1456.
[7] P. Pal, A. Pal, K. Nakashima, B.K. Yadav, Applications of chitosan in environmental remediation: a review, Chemosphere, 266 (2021) 128934, doi: 10.1016/j.chemosphere.2020.128934.
[8] M. Saranya, S. Latha, M.R.G. Reddi, T. Gomathi, P.N. Sudha, S. Anil, Adsorption studies of lead(II) from aqueous solution onto nanochitosan/polyurethane/polypropylene glycol ternary blends, Int. J. Biol. Macromol., 104 (2017) 1436–1448.
[9] Z. Ji, Y.S. Zhang, H.C. Wang, C.R. Li, Polypropylene glycol modified chitosan composite as a novel adsorbent to remove Cu(II) from wastewater, Tenside, Surfactants, Deterg., 58 (2021) 486–489.

[10] Y.R. Feng, B.S. Ma, X. Guo, H.B. Sun, Y.J. Zhang, H.Y. Gong, Preparation of amino-modified hydroxyapatite and its uranium adsorption properties, J. Radioanal. Nucl. Chem., 319 (2019) 437–446.
[11] Y.N. Chen, M.L. Li, Y.P. Li, Y.H. Liu, Y.R. Chen, H. Li, L.S.Z. Li, F.T. Xu, H.J. Jiang, L. Chen, Hydroxyapatite modified sludge-based biochar for the adsorption of Cu^{2+} and Cd^{2+}: adsorption behavior and mechanisms, Bioresour. Technol., 321 (2020) 124413, doi: 10.1016/j.biortech.2020.124413.
[12] W.J. Jiang, Q. Cai, W. Xu, M.W. Yang, Y. Cai, D.D. Dionysiou, K.E. O'Shea, Cr(VI) adsorption and reduction by humic acid coated on magnetite, Environ. Sci. Technol., 48 (2014) 8078–8085.
[13] Z.Z. Pan, X.M. Zhu, A. Satpathy, W.L. Li, J.D. Fortner, D.E. Gianmmar, Cr(VI) adsorption on engineered iron oxide nanoparticles: exploring complexation processes and water chemistry, Environ. Sci. Technol., 53 (2019) 11913–11921.
[14] Z. Ji, Y.S. Zhang, H.Y. Yan, B. Wu, B.C. Wei, Y.Y. Guo, H.C. Wang, C.R. Li, Adsorption of lead and tetracycline in aqueous solution by magnetic biomimetic bone composite, Polym. Bull., (2023), doi: 10.1007/s00289-023-04715-7.
[15] M.F. Shao, F.Y. Ning, J.W. Zhao, M. Wei, D.G. Evans, X. Duan, Preparation of Fe_3O_4@SiO_2@layered double hydroxide core-shell microspheres for magnetic separation of proteins, J. Am. Chem. Soc., 134 (2012) 1071–1077.
[16] B.Y. Huang, Y.G. Liu, B. Li, S.B. Liu, G.M. Zeng, Z.W. Zeng, X.H. Wang, Q.M. Ning, B.H. Zheng, C.P. Yang, Effect of Cu(II) ions on the enhancement of tetracycline adsorption by Fe_3O_4@SiO_2-chitosan/graphene oxide nanocomposite, Carbohydr. Polym., 157 (2017) 576–585.
[17] J.J. Cheng, G.H. Tan, W.T. Li, H.Y. Zhang, X.D. Wu, Z.Q. Wang, Y.X. Jin, Facile synthesis of chitosan assisted multifunctional magnetic Fe_3O_4@SiO_2@CS@pyropheophorbide-a fluorescent nanoparticles for photodynamic therapy, New J. Chem., 40 (2016) 8522–8534.
[18] R. Davarnejad, Z.K. Dastnayi, J.F. Kennedy, Cr(VI) adsorption on the blends of Henna with chitosan microparticles: experimental and statistical analysis, Int. J. Biol. Macromol., 116 (2018) 281–288.
[19] Y. Liu, S.H. Wu, C. Hua, X. Han, Effect of synergistic sorption of Cr(VI) and Mn(II) in aqueous solution using magnetic nanoparticles, Desal. Water Treat., 52 (2014) 4183–4189.
[20] X.B. Fan, X.H. Wang, Y.T. Cai, H.H. Xie, S.Q. Han, C. Hao, Functionalized cotton charcoal/chitosan biomass-based hydrogel for capturing Pb^{2+}, Cu^{2+} and MB, J. Hazard. Mater., 423 (2022) 127191, doi: 10.1016/j.jhazmat.2021.127191.
[21] R.H. Huang, B.C. Yang, B. Wang, D.S. Zheng, Z.Q. Zhang, Removal of chromium(VI) ions from aqueous solutions by N-2-hydroxypropyl trimethyl ammonium chloride chitosan-bentonite, Desal. Water Treat., 50 (2012) 329–337.
[22] M. Mirabedini, M.Z. Kassaee, Removal of toxic Cr(VI) from water by a novel magnetic chitosan/glyoxal/PVA hydrogel film, Desal. Water Treat., 57 (2016) 14266–14279.
[23] C.F. Zheng, H.L. Zheng, Y.J. Wang, Y.L. Wang, W.Q. Qu, Q. An, Y.Z. Liu, Synthesis of novel modified magnetic chitosan particles and their adsorption performance toward Cr(VI), Bioresour. Technol., 267 (2018) 1–8.
[24] J.L. Wang, X. Guo, Adsorption isotherm models: classification, physical meaning, application and solving method, Chemosphere, 258 (2020) 127279, doi: 10.1016/j.chemosphere.2020.127279.
[25] S. Hussain, M. Kamran, S.A. Khan, K. Shaheen, Z. Shah, H. Suo, Q. Khan, A.B. Shah, W.U. Rehman, Y.O. Al-Ghamdi, U. Ghani, Adsorption, kinetics and thermodynamics studies of methyl orange dye sequestration through chitosan composites films, Int. J. Biol. Macromol., 168 (2021) 383–394.
[26] H. Wang, W.C. Wang, S. Zhou, X.C. Gao, Adsorption mechanism of Cr(VI) on woody-activated carbons, Heliyon, 9 (2023) e13267, doi: 10.1016/j.heliyon.2023.e13267.
[27] H. Zhang, R. Xiao, R.H. Li, A. Ali, A.L. Chen, Z.Q. Zhang, Enhanced aqueous Cr(VI) removal using chitosan-modified magnetic biochars derived from bamboo residues, Chemosphere, 261 (2020) 127694, doi: 10.1016/j.chemosphere.2020.127694.
[28] S.M. Anush, H.R. Chandan, B.H. Gayathri, Asma, N. Manju, B. Vishalakshi, B. Kalluraya, Graphene oxide functionalized chitosan-magnetite nanocomposite for removal of Cu(II) and Cr(VI) from waste water, Int. J. Biol. Macromol., 164 (2020) 4391–4402.
[29] X. Peng, Z.C. Yan, L.H. Hu, R.Z. Zhang, S.J. Liu, A.L. Wang, X.W. Yu, L. Chen, Adsorption behavior of hexavalent chromium in aqueous solution by polyvinylimidazole modified cellulose, Int. J. Biol. Macromol., 155 (2020) 1184–1193.
[30] Y.B. Feng, Y. Du, Z.T. Chen, M.X. Du, K. Yang, X.J. Lv, Z.F. Li, Synthesis of Fe_3O_4 nanoparticles with tunable sizes for the removal of Cr(VI) from aqueous solution, J. Coat. Technol. Res., 15 (2018) 1145–1155.
[31] T.R.S. Cadaval, A.S. Camara, G.L. Dotto, L.A.D. Pinto, Adsorption of Cr(VI) by chitosan with different deacetylation degrees, Desal. Water Treat., 51 (2013) 7690–7699.
[32] Y.L. Jiang, M.R. Abukhadra, N.M. Refay, M.F. Sharaf, M.A. El-Meligy, E.M. Awwad, Synthesis of chitosan/MCM-48 and β-cyclodextrin/MCM-48 composites as bio-adsorbents for environmental removal of Cd^{2+} ions; kinetic and equilibrium studies, React. Funct. Polym., 154 (2020) 104675, doi: 10.1016/j.reactfunctpolym.2020.104675.
[33] X.Y. Zhou, X. Zhou, The unit problem in the thermodynamic calculation of adsorption using the Langmuir equation, Chem. Eng. Commun., 201 (2014) 1459–1467.
[34] E.C. Lima, A.A. Gomes, H.N. Tran, Comparison of the nonlinear and linear forms of the van't Hoff equation for calculation of adsorption thermodynamic parameters ($\Delta S°$ and $\Delta H°$), J. Mol. Liq., 311 (2020) 113315, doi: 10.1016/j.molliq.2020.113315.
[35] H.N. Tran, S.J. You, A. Hosseini-Bandegharaei, H.P. Chao, Mistakes and inconsistencies regarding adsorption of contaminants from aqueous solutions: a critical review, Water Res., 120 (2017) 88–116.
[36] H.N. Tran, S.J. You, H.P. Chao, Thermodynamic parameters of cadmium adsorption onto orange peel calculated from various methods: a comparison study, J. Environ. Chem. Eng., 4 (2016) 2671–2682.
[37] B. Choudhary, D. Paul, A. Singh, T. Gupta, Removal of hexavalent chromium upon interaction with biochar under acidic conditions: mechanistic insights and application, Environ. Sci. Pollut. Res., 24 (2017) 16786–16797.